

## Stokes–anti-Stokes correlated photon properties akin to photonic Cooper pairs


Filomeno S. de Aguiar Júnior,<sup>1</sup> André Saraiva,<sup>2</sup> Marcelo F. Santos,<sup>2</sup> Belita Koiller,<sup>2</sup> Reinaldo de Melo e Souza,<sup>3</sup> Arthur Patrocínio Pena,<sup>1</sup> Raigna A. Silva,<sup>1,4</sup> Carlos H. Monken,<sup>1</sup> and Ado Jorio<sup>1,\*</sup>

<sup>1</sup>*Departamento de Física, UFMG, Belo Horizonte, MG 31270-901, Brazil*

<sup>2</sup>*Instituto de Física, UFRJ, Caixa Postale 68528, Rio de Janeiro, RJ 21941-972, Brazil*

<sup>3</sup>*Instituto de Física, UFF, Niterói, RJ 24210-346, Brazil*

<sup>4</sup>*Instituto de Física, UFU, Uberlândia, MG, Brazil*

 (Received 5 October 2018; revised manuscript received 21 December 2018; published 13 March 2019)

Photons interact with each other in condensed matter through the same mechanism that forms Cooper pairs in superconductors—the exchange of virtual phonons [A. Saraiva *et al.*, *Phys. Rev. Lett.* **119**, 193603 (2017)]. It is, however, unclear which consequences of this interaction will be observable and potentially lead to further analogy with superconductivity. We investigate the energy, momentum, and production rate of correlated Stokes–anti-Stokes (SaS) photons in diamond and other transparent media, experiencing properties akin to those of electronic Cooper pairs. The rate of correlated SaS production depends on the energy shifts of the pair, which in the BCS theory determines whether there should be an attractive or repulsive interaction. With this view, we only observe correlated SaS in the case of attractive interactions. While traditional photon-phonon collisions scatter light in all directions, the correlated SaS photons follow the same path as the noninteracting laser. The observed correlated SaS photon pairs are rare, but our model indicates paths to achieve higher interaction energies.

DOI: [10.1103/PhysRevB.99.100503](https://doi.org/10.1103/PhysRevB.99.100503)

The production of red-shifted (Stokes) and blue-shifted (anti-Stokes) photons by inelastic scattering of light in matter, where the incoming laser photons of energy  $E_L = \hbar\omega_L$  may lose or gain energy in the form of atomic vibrations (phonons) of energy  $E_q$ , is known as Raman scattering [1,2] and it is used for characterizing materials properties in materials science studies [3]. By selecting detection events that happen within a short time interval (femtosecond to picosecond range) [4] and symmetrically shifted in frequency from the excitation laser mode, we are able to identify correlated Stokes–anti-Stokes (SaS) photon pairs [5]. They come from events in which the same phonon created in the sample by the Stokes (S) process is annihilated by the anti-Stokes (aS) process [6,7]. Several recent studies [5,8–12] explored the production of SaS pairs through real processes, i.e., when the energy (Raman) shifts  $\varepsilon_{aS}$  and  $\varepsilon_S$  correspond, respectively, to plus and minus a quantum of vibration  $E_q$  in the material (resonant process). Their main motivation is the potential applications of SaS pairs in quantum information.

The production of SaS photon pairs may occur out of resonance ( $|\varepsilon_{S,aS}| \neq E_q$ ,  $\varepsilon_S = -\varepsilon_{aS}$  for energy conservation), in a process we call virtual SaS, viewed as the photonic counterparts of superconducting Cooper pairs [13–15]. An analogy between the virtual SaS and photonic Cooper pairs (PCPs) was then proposed [14], but there is so far no exploration of the properties akin to those of PCPs [13] and photonic four-wave mixing [16–18].

In the second quantization, any two-particle interaction Hamiltonian can be described in the form [19]

$$\hat{H}_{\text{int}} = \sum_{\mathbf{k}_1, \mathbf{k}_2, \mathbf{k}_3, \mathbf{k}_4} V(\mathbf{k}_1, \mathbf{k}_2, \mathbf{k}_3, \mathbf{k}_4) \hat{a}_{\mathbf{k}_4}^\dagger \hat{a}_{\mathbf{k}_3}^\dagger \hat{a}_{\mathbf{k}_2} \hat{a}_{\mathbf{k}_1}, \quad (1)$$

where  $\mathbf{k}_i$  labels the quantum states. This  $\hat{H}_{\text{int}}$  can be used to describe electron-electron coupling in superconductivity, nonlinear photon-photon processes, and any two-particle interaction phenomenon, with the specificities residing in the interaction potential  $V(\mathbf{k}_1, \mathbf{k}_2, \mathbf{k}_3, \mathbf{k}_4)$ . All such processes represent four-wave mixing, although this terminology is generally used only in the field of optics [20], where  $V(\mathbf{k}_1, \mathbf{k}_2, \mathbf{k}_3, \mathbf{k}_4)$  is associated with a third-order electrical susceptibility.

A billiardlike picture representing such a photon-photon interaction is depicted in Fig. 1(a). This process is implemented experimentally with the incoming laser beam focused inside a diamond slab of 1.7 mm by a microscope objective of low numerical aperture (NA = 0.6), and the forward scattered light collimated by another microscope objective of high NA = 0.9 in a confocal arrangement [21]. The sample is excited with a  $T_L = 200$ -fs-width pulsed laser at  $R_L = 76$  MHz pulse rate, wavelength  $\lambda_L = 633$  nm, and the PCPs are selected by time filtering only S and aS photons that arrive in two different photon counters (avalanche photodiodes – APDs) in the same laser pulse (time delay  $\Delta t = 0$  [21]). Accidental coincidences also happen (uncorrelated S and aS photons measured at  $\Delta t = 0$ ) [22], and they can be filtered considering the correlated SaS count rate given by

$$I_{SaS}^{\text{corr}} = I_{SaS}(\Delta t = 0) - \overline{I_{SaS}}(\Delta t \neq 0), \quad (2)$$

where the overline indicates average over the measured SaS count rate  $I_{SaS}(\Delta t \neq 0)$ , valid because for coherent fields the normalized second-order correlation function  $g^2(\Delta t = 0) = I_{SaS}(\Delta t = 0)/\overline{I_{SaS}}(\Delta t \neq 0) = 1$ .

Figure 1(b) shows  $I_{SaS}^{\text{corr}}$  (black circles) for different values of  $\varepsilon_S$  and  $\varepsilon_{aS}$ . A single experimental detection measures the number of S and aS photon pairs reaching the two APDs at the same time ( $\Delta t = 0$ ), counting during 600 s, and the same

\*Corresponding author: [adojorio@fisica.ufmg.br](mailto:adojorio@fisica.ufmg.br)

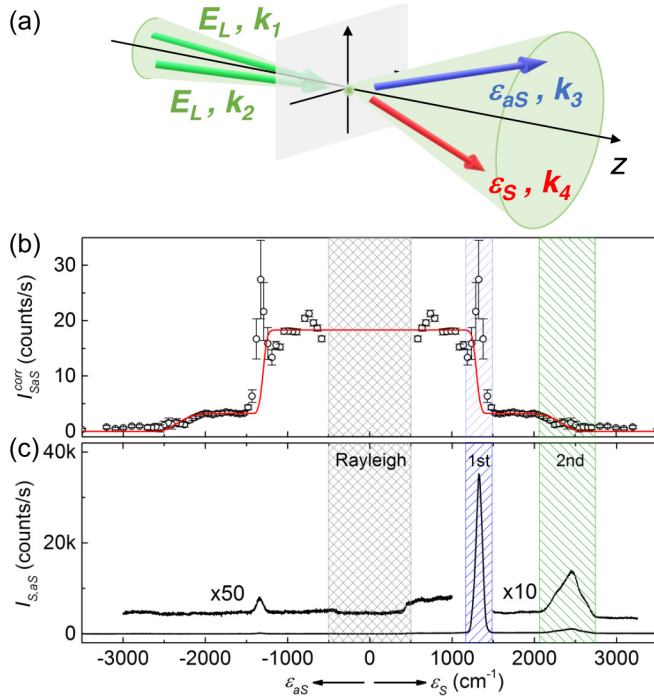


FIG. 1. (a) Schematics showing light-by-light scattering. (b) The black circles span the number of correlated SaS measured per second, under the excitation power of  $P_L = 40$  mW. The error bars are taken as the sum of  $\sqrt{N}$  (per second) for  $I_{SaS}(\Delta t = 0)$  and  $\bar{I}_{SaS}(\Delta t \neq 0)$ , where  $N$  is the total number of events observed during 600 s accumulation time per data point. The red line is a fitting to the data considering Eq. (4). (c) The black solid line gives the Raman spectrum.

data point is represented twice, in both  $\epsilon_S$  and  $\epsilon_{aS}$  sides of the graphic. Only the S beam is spectrally filtered using a monochromator ( $26 \text{ cm}^{-1}$  resolution) to simplify the spectral filtering dependence, since we have already established that the correlated SaS only exists for  $\epsilon_S = -\epsilon_{aS}$  [5,14]. The accidental coincidences depend on whether the aS beam is filtered or not, but this is irrelevant for the correlated SaS counting.

In Figure 1(c) the black line gives the Raman intensity  $I_{S,aS}(\epsilon_S, \epsilon_{aS})$  of the sample, measured with a spectrometer equipped with a charge coupled device (CCD). The result is quantitatively consistent with the  $I_{S,aS}(\epsilon_S, \epsilon_{aS})$  measured with one APD replacing the CCD and using the spectrometer as a monochromator. We adopt the usual convention in Raman spectroscopy, representing the Stokes shift in the plot as positive [ $\epsilon_S = -(E_L - E_S)$ ], while  $\epsilon_{aS} = -(E_L - E_{aS}) < 0$ ]. The black-hatched area indicates the Rayleigh spectral region, removed with a notch filter, and the blue- and green-hatched areas in the Stokes side indicate the ranges of first-order and second-order Raman spectral responses, respectively [21].

From panels (b) and (c) in Fig. 1 we conclude that  $I_{SaS}^{corr}(\epsilon_S, \epsilon_{aS})$  is highest for pairs formed by virtual phonons with  $|\epsilon_S, \epsilon_{aS}| < E_{q=0} = 1332 \text{ cm}^{-1}$  [23], dropping significantly once this first-order Raman peak is crossed. Correlated SaS are also observed, with lower count rates, between  $E_{q=0}$  and the second-order (two-phonon scattering, with  $+q$  and  $-q$  nonzero momenta) Raman feature at  $2E_q = 2500 \text{ cm}^{-1}$ , which comes from a peak at  $E_{q \neq 0} \sim 1250 \text{ cm}^{-1}$  in the di-

among phonon density of states [23], and  $I_{SaS}^{corr}$  drops again when crossing the second-order Raman peak.

The energy behavior in the correlated SaS efficiency can be explained using Eq. (1) to investigate the quantum state  $|\psi_f\rangle$  of the outgoing correlated SaS, where  $\mathbf{k}_i$  labels the four-photon momenta [see Fig. 1(a)] ( $i = 1, 2$ ) for the incident (laser) photons and ( $i = 3, 4$ ) for the scattered (aS and S) photons, and  $\hat{a}_{\mathbf{k}_i}$  are photon annihilation operators [14].  $|\psi_f\rangle = e^{-i\hat{H}_{int}t}|\psi_0\rangle \sim (\mathbf{1} + i\hat{H}_{int}dt/\hbar)|\psi_0\rangle$ , with  $|\psi_0\rangle = |\alpha_L\rangle|00\rangle$ , where  $|\alpha_L\rangle$  represents the coherent laser state, and  $|00\rangle$  the S and aS vacuum state. The correlated SaS are produced mainly with the same polarization of the incident laser [5]; however, for simplicity, we do not consider polarization here.

The  $I_{SaS}^{corr}(\epsilon_S, \epsilon_{aS})$  is due to spontaneous Raman scattering, driven by the vacuum of phonon, S, and aS photon fields. This is the case because in the maximum (resonant) observed value of  $I_S(\epsilon_S = 1332 \text{ cm}^{-1}) \sim 35$  kilocounts/s [see Fig. 1(c)], the probability to generate a Stokes photon in one pulse is  $10^{-4}$ , and much less for aS. The phonon lifetimes (femtosecond to picosecond range) are much shorter than the time distance between pulses (13 ns), so that the correlated SaS production happens necessarily within one pulse, which is with a very high probability in the vacuum state of S photons, of aS photons, and of phonons (for diamond  $E_q$  is much higher than the room temperature thermal energy).

The most important aspect in Fig. 1 is the roughly constant correlated SaS rate in energy, but highly asymmetric with respect to the resonant processes, which take place at the Raman-active phonon energies  $E_{q=0}$  and  $2E_{q \neq 0}$  in the first- and second-order scattering processes, respectively. The energy dependence of the perturbative photon-photon coupling  $V(\mathbf{k}_1, \mathbf{k}_2, \mathbf{k}_3, \mathbf{k}_4)$ , as obtained in Ref. [14], describes a correlated SaS production rate that is symmetric with respect to the phonon energy  $E_q$ , and it does not fit the data. Other possibilities, such as losses (e.g., phonon decay), resonant and nonresonant Raman contributions, or quantum interference between the first- and second-order Raman processes have also been considered, but they are not able to fit the data due to the relatively large asymmetry of the correlated SaS production rate above and below the Raman peak together with the relatively sharp (in width) and symmetric Raman peak. Therefore, within the perturbative quantum mechanics framework introduced in Ref. [14] the  $I_{SaS}^{corr}$  dependence on  $|\epsilon_S, \epsilon_{aS}|$  is inexplicable. Notice that the results and consequences of the BCS theory of superconductivity cannot be obtained within a perturbation theory framework based on unpaired unperturbed electrons, even if summed over all orders.

Akin to the BCS original theory [24], we adopt here the simplified description of the interaction potential

$$V(\mathbf{k}_1, \mathbf{k}_2, \mathbf{k}_3, \mathbf{k}_4) = \begin{cases} -V_0, & |\epsilon_S, \epsilon_{aS}| < E_q, \\ 0, & |\epsilon_S, \epsilon_{aS}| > E_q, \end{cases} \quad (3)$$

i.e., a negative constant coupling between two photons when their SaS Raman shift modulus is less than the energy of a real phonon, and zero elsewhere [25]. Thus,  $V(\mathbf{k}_1, \mathbf{k}_2, \mathbf{k}_3, \mathbf{k}_4)$  of Eq. (3) implies that correlated SaS are formed in the attractive interaction range. The virtual particle mediating this interaction exists only during the very short time interval ( $\lesssim 10$  fs)

in which the photons coexist inside the  $\sim 3 \mu\text{m}$  focal region of the pump laser beam, in a genuine photon-photon collision conserving energy and momentum. As for the familiar BCS Cooper pairs, photons deviated by energies corresponding to positive values of  $V(\mathbf{k}_1, \mathbf{k}_2, \mathbf{k}_3, \mathbf{k}_4)$  interact repulsively and we empirically conclude that they do not form correlated SaS. We may write the Raman shift dependence of the correlated SaS production rate as [21]

$$I_{SaS}^{\text{corr}} = \Delta k \left| \alpha_L^2 V_0 \frac{T_L}{\hbar} \right|^2 R_L, \quad (4)$$

for  $|\varepsilon_{S,aS}| < E_q$ , where  $|\alpha_L|^2$  is the number of pump laser photons per pulse ( $1.8 \times 10^9$  for  $P_L = 40 \text{ mW}$ ), and  $\Delta k$  is the spectral collection obtained experimentally from the ratio between the monochromator resolution and the total scattering range of nonzero potential ( $1332 \text{ cm}^{-1}$  for first order and  $2500 \text{ cm}^{-1}$  for second order). Solid angle is not considered here because, as shown later, the correlated SaS cross the sample without momentum scattering. Since the interaction is mediated by phonons, the value of  $V_0$  is proportional to the electron-phonon scattering efficiency squared  $M_q^2$  [14], and it can be obtained directly from the Raman-scattering intensity  $I_S \propto M_q^2$ , then  $|V_0^{1\text{st},2\text{nd}}| = C^{1\text{st},2\text{nd}} A_S^{1\text{st},2\text{nd}}$ , where  $A_S^{1\text{st},2\text{nd}}$  is the area below the Stokes first- and second-order Raman peaks, obtained experimentally from Fig. 1(c).  $I_{SaS}^{\text{corr}}(\varepsilon_{S,aS})$  according to Eq. (4) is shown by the red solid line in Fig. 1(b), with the fitting parameters  $C^{1\text{st}} = 5.75 \times 10^{-22}$  and  $C^{2\text{nd}} = 3.35 \times 10^{-21}$ , in units of  $[\text{eV cm s}]$ , adjusting the intensity levels below and above  $1332 \text{ cm}^{-1}$ .

Another interesting property of the emerging correlated SaS is given by momentum conservation (or photonic phase matching), where the billiardlike physics resulting from this interaction may be probed analyzing the transverse spatial correlation of the pairs, as depicted in Fig. 2. The angular spread of the scattered photons is analyzed by limiting the solid angle collected by the detection system with the help of a circular aperture (iris) of variable radius  $r$ , as shown schematically in Fig. 2(a).

Typically, photons ricochet in all directions when they scatter against phonons, resulting in an intensity profile for the Raman effect with a deviation from the forward propagation direction of the incident laser beam [26]. This is evidenced by the steady growth of the count rate of scattered aS and S photons as a function of the iris aperture shown by the red and blue crossed circles, respectively, in Fig. 2(b).

In contrast, the nonresonant correlated SaS count [green stars in Fig. 2(b)] inherits the same spatial profile defined by the excitation laser [green crossed circles in Fig. 2(b)], dropping significantly only when the iris is closed below  $r = 2 \text{ mm}$ . For resonant SaS, where accidental coincidences are significant,  $I_{SaS}^{\text{corr}}$  (open black stars) follows the laser dependence, while accidental coincidences (filled black stars) follow the unpaired aS and S photons tendency. Therefore, although the accidental coincidences are correlated in time, they belong to uncorrelated scattering processes, in other words, they are not correlated SaS. The correlated SaS cross the material following the same path as the noninteracting incident laser—a phenomenon analogous to the transfer of amplitude profile in spontaneous parametric down conver-

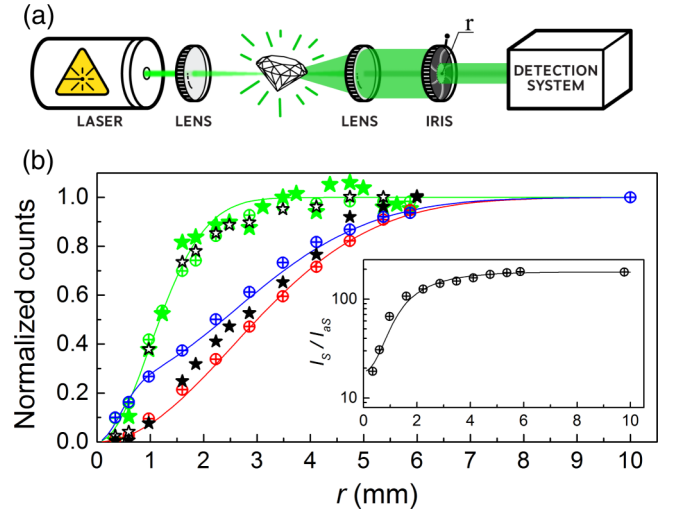


FIG. 2. (a) Angular spread for inelastic scattered light emerging after crossing a diamond slab, analyzed by recollimating the scattered rays with a confocal lens and selectively blocking the outer rays with a variable radius aperture  $r$  (iris). (b) Normalized iris aperture dependence for the unpaired S intensities (red crossed circles); unpaired aS intensities (blue crossed circles); noninteracting excitation laser (green crossed circles); time correlated SaS photon pairs (green and black stars). The unpaired S and aS signals are collected at the real Raman peak energies ( $\varepsilon_{S,aS} = \pm 1332 \text{ cm}^{-1}$ ). The SaS correlated photons are collected both at the Raman peak energy ( $\varepsilon_{S,aS} = \pm 1332 \text{ cm}^{-1}$ ; open and filled black stars) and outside ( $\varepsilon_{S,aS} = \pm 900 \text{ cm}^{-1}$ ; green stars), to select SaS pairs created by real and virtual phonons, respectively. For the real SaS we plot separately the true coincidences (correlated SaS; open symbols) and the accidental coincidences (filled symbols); the total counts  $I_{SaS}(\Delta t = 0)$  (not shown) fall in between the two. The inset plots the ratio between the unpaired S and aS intensities measured at  $\varepsilon_{S,aS} = \pm 1332 \text{ cm}^{-1}$ . Solid lines are fitting to the data.

sion [21,27–29], a hint for establishing photonic supercurrent behavior.

The data in Fig. 2(b) can be fitted considering a Gaussian distribution of the scattered intensities (solid lines [21]). Regarding the real aS data [blue crossed circles in Fig. 2(b)], good fits are obtained considering a sum of two Gaussian distributions. This phenomenon is better visualized considering the intensity ratio  $I_S/I_{aS}$  between the unpaired S and aS signals, shown in the inset to Fig. 2(b). This ratio provides a figure of merit for both the thermally and the correlated SaS generated aS signals playing a role in the observed scattering [7]. The significant decay in  $I_S/I_{aS}$  for  $r < 2 \text{ mm}$  demonstrates the aS Raman signal is dominated by the correlated SaS in the low scattering angle region, providing a spatial-filter technique to reject uncorrelated S and aS signals.

Interestingly, the demonstration of momentum and energy conservation in this light-by-light scattering process is straightforward for each correlated SaS pair [14], while electronic Cooper pairs exist as a collective state inside superconductors, defying any attempts to address each pair individually. On the other hand, photon-photon interactions mediated by vacuum fluctuations are notoriously faint; for instance, in the Atlas experiments, such interactions are observable, but only under very special conditions [30], in the really very

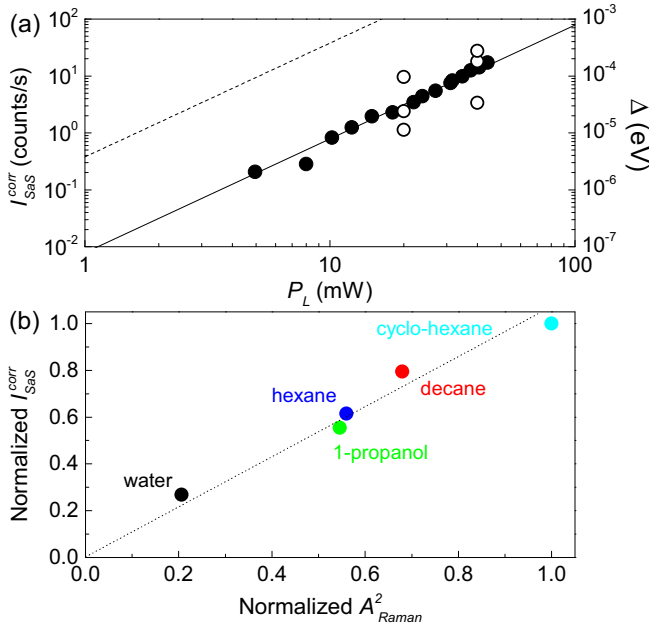


FIG. 3. (a) Correlated SaS rate  $I_{SaS}^{corr}$  as a function of excitation laser power ( $P_L$ ). The black circles following the solid line are measurements for diamond with a Raman shift of  $\varepsilon_{S,as} = \pm 900 \text{ cm}^{-1}$ . For  $P_L = 20$  and  $40 \text{ mW}$  (see open circles),  $I_{SaS}^{corr}$  are also obtained at three different Raman shifts, namely,  $\pm 1700 \text{ cm}^{-1}$  (above  $E_{q=0}$ ),  $\pm 900 \text{ cm}^{-1}$  (below  $E_{q=0}$ ), and  $\pm 1332 \text{ cm}^{-1}$  (at  $E_{q=0}$ ), from lower to higher  $I_{SaS}^{corr}$  values, respectively. The right axis is the calculated interaction energy  $\Delta$  stemming from the count rate. The dashed line is the expected interaction energy for the twisted bilayer graphene, estimated from the enhancement in SaS processes relative to diamond obtained in Ref. [7]. (b)  $I_{SaS}^{corr}(\varepsilon_{S,as} = \pm 2070 \text{ cm}^{-1})$  as a function of the relative Raman cross section above  $\varepsilon_{S,as}$ , for different hydrocarbons and water, all measured with  $P_L \sim 30 \text{ mW}$ . The relative Raman cross sections are estimated from the squared Raman peak area,  $A_{Raman}^2$ . All matrix elements and correlated SaS rates are taken as compared to the highest measured matrix element (cyclohexane).

high energies regime. As a result, the number of observed correlated SaS is extremely small, approximately one pair for every  $10^{15}$  incident photons. We here observe a rate of approximately 20 correlated SaS per second for Raman shifts below  $1300 \text{ cm}^{-1}$  in Fig. 1(b). This rate is proportional to the interaction energy, which is the main energy scale that will determine if other analogous effects related to superconductivity will be observable. We estimate the interaction energy for photons scattered by diamond phonons at a Raman shift of  $\varepsilon_{S,as} = \pm 900 \text{ cm}^{-1}$  from the transition probability  $p = |\Delta|^2 dt^2 / \hbar^2$  [21], where  $\Delta = V_0 |\alpha_L|^2$  is the transition amplitude [14]. We conclude that  $\Delta \gtrsim 10 \mu\text{eV}$  and then estimate an average attractive interaction energy  $V_0 \approx 10 \text{ feV}$  for diamond under our experimental conditions.

Considering the dependence of the interaction  $\Delta$  with the laser power ( $P_L = |\alpha_L|^2 \hbar \omega_L R_L$ ), in Fig. 3(a) we estimate how large this interaction strength may become if a more intense laser is used. The rate of pair production (filled circles) is proportional to the squared laser power ( $P_L^2$ ), but with the absolute value depending on whether the frequency shift is below, at, or above the phonon resonance (see open circles measured at two different  $P_L$  values). Another parameter that

may be explored in order to enhance  $\Delta$  is the efficiency of the Raman scattering  $M_q$ . The intensity of pairs should, therefore, be also proportional to the squared Raman peak area  $A_{Raman}^2$ . We confirm this relationship by plotting  $I_{SaS}^{corr}(\varepsilon_{S,as} = \pm 2070 \text{ cm}^{-1})$  as a function of the experimentally obtained  $A_{Raman}^2$  above  $\varepsilon_{S,as}$  in different hydrocarbons and water [see Fig. 3(b)]. The listed materials are chosen here because they all exhibit a Raman peak near  $2900 \text{ cm}^{-1}$  (C-H and O-H vibrations) and no other Raman-scattering contribution down to  $\sim 2070 \text{ cm}^{-1}$ . The observation of  $I_{SaS}(\varepsilon_{S,as}) \propto A_{Raman}^2$  in different materials is an ultimate proof that phonons are indeed responsible for the photon-photon scattering.

For completeness, we have measured the  $\varepsilon_{S,as}$  dependence of  $I_{SaS}^{corr}(\varepsilon_{S,as})$  for one liquid (decane, not shown) and, consistently, we could not observe correlated SaS above the highest frequency Raman mode at  $\sim 2900 \text{ cm}^{-1}$ . Therefore, the  $I_{SaS}^{corr}(\varepsilon_{S,as})$  asymmetry with respect to the phonon energy holds for both solids and liquids, indicating the universality of the correlated SaS phenomenon. The fact that virtually any transparent medium will generate pairs suggests that the photon pairs may be tailored in all its properties, such as energy, polarization, momentum, and phase, by suitable choices of materials. Moreover, the input light source may be of any kind, as long as it is strong enough to actually generate pairs, and the consequences of the supercurrent analogy will serve as a basis for new application proposals. The simplest of these consequences is the iris experiment (Fig. 2), which shows the S and aS photons crossing the material without the spread usually observed in light-phonon scattering. Similarly, there could be no spread in propagation time. Like in electronic superconductivity, these entanglement-derived properties should be a source of photonic state stability.

In our diamond experiment, typical orders of magnitude for the laser energy  $E_L$ , real phonon energies  $E_q$ , and transition amplitude  $\Delta$  are 1, 0.1, and  $10^{-5} \text{ eV}$ , respectively. Shen *et al.* [13] identify the phonon energy as the superconducting gap. We speculate that if a transition amplitude  $\Delta$  reaches the phonon  $E_q$  or the photon  $E_L$  energies, new physical phenomena may happen. Specifically, the relation between the formation of the pairs and the vibration of the material points in the direction of using this technique to explore the material's properties beyond the information provided by standard intensity measurements. A more radical rupture would be the observation of speed of light renormalization, lending photons some finite mass, which would be central to the prediction of what collective bosonic condensate state (photonic liquid) might emerge.

More efficient Raman scattering is needed in order to explore the meaning and usefulness of  $\Delta$ . For instance, a coincidence rate increase by a factor of 390 for resonant SaS pairs was obtained in twisted bilayer graphene by engineering van Hove singularities [31]. This may lead to interactions of the order of meV, as shown by the dashed line in Fig. 3(a). Clearly, other experimental studies and a microscopic theory are needed for further advances.

We acknowledge L. M. Malard for helpful discussions and C. Rabelo for technical assistance. Financial support from CNPq (Grants No. 552124/2011-7, No. 307481/2013-1, No. 304869/2014-7, No. 460045/2014-8,

No. 305384/2015-5, and No. 309861/2015-2), FINEP (Grant No. 01.13.0330.00), CAPES (RELAI), and FAPERJ

(Grants No. E-26/202.915/2015 and No. E-05/2016tTXE-05/2016).

- 
- [1] C. V. Raman and K. S. Krishnan, *Nature (London)* **121**, 501 (1928).
- [2] D. F. Walls, *Z. Physik* **237**, 224 (1970).
- [3] H. Kuzmany, *Solid-State Spectroscopy: An Introduction* (Springer Science & Business Media, Berlin, 2009).
- [4] E. del Valle, A. Gonzalez-Tudela, F. P. Laussy, C. Tejedor, and M. J. Hartmann, *Phys. Rev. Lett.* **109**, 183601 (2012).
- [5] M. Kasperczyk, F. S. de Aguiar Júnior, C. Rabelo, A. Saraiva, M. F. Santos, L. Novotny, and A. Jorio, *Phys. Rev. Lett.* **117**, 243603 (2016).
- [6] D. Klyshko, *Quantum Electron.* **7**, 755 (1977).
- [7] C. A. Parra-Murillo, M. F. Santos, C. H. Monken, and A. Jorio, *Phys. Rev. B* **93**, 125141 (2016).
- [8] K. C. Lee, M. R. Sprague, B. J. Sussman, J. Nunn, N. K. Langford, X.-M. Jin, T. Champion, P. Michelberger, K. F. Reim, D. England *et al.*, *Science* **334**, 1253 (2011).
- [9] K. Lee, B. Sussman, M. Sprague, P. Michelberger, K. Reim, J. Nunn, N. Langford, P. Bustard, D. Jaksch, and I. Walmsley, *Nat. Photonics* **6**, 41 (2012).
- [10] D. G. England, P. J. Bustard, J. Nunn, R. Lausten, and B. J. Sussman, *Phys. Rev. Lett.* **111**, 243601 (2013).
- [11] R. Riedinger, S. Hong, R. A. Norte, J. A. Slater, J. Shang, A. G. Krause, V. Anant, M. Aspelmeyer, and S. Gröblacher, *Nature (London)* **530**, 313 (2016).
- [12] M. D. Anderson, S. Tarrago Velez, K. Seibold, H. Flayac, V. Savona, N. Sangouard, and C. Galland, *Phys. Rev. Lett.* **120**, 233601 (2018).
- [13] J. Q. Shen, H. Y. Zhu, and H. L. Zhu, *Laser & Infrared (in Chinese)* **32**, 315 (2002).
- [14] A. Saraiva, F. S. de Aguiar Júnior, R. de Melo e Souza, A. P. Pena, C. H. Monken, M. F. Santos, B. Koiller, and A. Jorio, *Phys. Rev. Lett.* **119**, 193603 (2017).
- [15] Y. Zhang, L. Zhang, and Y.-Y. Zhu, *Phys. Rev. A* **98**, 013824 (2018).
- [16] J. Fan, A. Migdall, J. Chen, and E. A. Goldschmidt, *IEEE J. Sel. Top. Quantum Electron.* **15**, 1724 (2009).
- [17] H. Takesue, *IEEE J. Sel. Top. Quantum Electron.* **18**, 1722 (2012).
- [18] L. Caspani, C. Xiong, B. J. Eggleton, D. Bajoni, M. Liscidini, M. Galli, R. Morandotti, and D. J. Moss, *Light: Sci. Appl.* **6**, e17100 (2017).
- [19] L. E. Ballentine, *Quantum Mechanics: A Modern Development*, 2nd ed. (World Scientific, Singapore, 2014).
- [20] R. W. Boyd, *Nonlinear Optics*, 3rd ed. (Academic, New York, 2003), p. 578.
- [21] See Supplemental Material at <http://link.aps.org/supplemental/10.1103/PhysRevB.99.100503> for (i) detailed information on the experimental setup; (ii) exemplary data for the SaS measurement in diamond; (iii) details on the fitting procedure for the iris experiment; (iv) details on the system efficiency and data correction; (v) formula for collision probability; and (vi) formalism for four-photon momentum conservation.
- [22] M. Kasperczyk, A. Jorio, E. Neu, P. Maletinsky, and L. Novotny, *Opt. Lett.* **40**, 2393 (2015).
- [23] S. A. Solin and A. K. Ramdas, *Phys. Rev. B* **1**, 1687 (1970).
- [24] J. Bardeen, L. N. Cooper, and J. R. Schrieffer, *Phys. Rev.* **108**, 1175 (1957).
- [25] O. Madelung, *Introduction to Solid-State Theory* (Springer Science & Business Media, Berlin, 2012), Vol. 2.
- [26] M. Schlösser, T. M. James, S. Fischer, R. J. Lewis, B. Bornschein, and H. H. Telle, *J. Raman Spectrosc.* **44**, 453 (2013).
- [27] D. C. Burnham and D. L. Weinberg, *Phys. Rev. Lett.* **25**, 84 (1970).
- [28] V. Boyer, A. M. Marino, R. C. Pooser, and P. D. Lett, *Science* **321**, 544 (2008).
- [29] S. Walborn, C. Monken, S. Pádua, and P. Souto Ribeiro, *Phys. Rep.* **495**, 87 (2010).
- [30] Atlas Collaboration, *Nat. Phys.* **13**, 852 (2017).
- [31] A. Jorio, M. Kasperczyk, N. Clark, E. Neu, P. Maletinsky, A. Vijayaraghavan, and L. Novotny, *Nano Lett.* **14**, 5687 (2014).